Mon. Not. R. Astron. Soc. **394,** 2098–2108 (2009) doi:10.1111/j.1365-2966.2009.14477.x

The evolution of the red sequence slope in massive galaxy clusters

J. P. Stott,[1,2⋆] K. A. Pimbblet,[3] A. C. Edge,[2] G. P. Smith[4,5] and J. L. Wardlow[2]

[1]*Astrophysics Research Institute, Liverpool John Moores University, Twelve Quays House, Egerton Wharf, Birkenhead, CH41 1LD*
[2]*Institute for Computational Cosmology, Department of Physics, University of Durham, South Road, Durham DH1 3LE*
[3]*Department of Physics, University of Queensland, Brisbane, QLD 4072, Australia*
[4]*California Institute of Technology, Mail Code 105-24, Pasadena, CA 91125, USA*
[5]*School of Physics & Astronomy, University of Birmingham, Edgbaston, Birmingham B15 2TT*

Accepted 2009 January 7. Received 2009 January 7; in original form 2008 June 17

ABSTRACT

We investigate the evolution of the optical and near-infrared colour–magnitude relation in an homogeneous sample of massive clusters from $z = 1$ to the present epoch. By comparing deep *Hubble Space Telescope* Advanced Camera for Surveys imaging of X-ray selected MAssive Cluster Survey (MACS) clusters at $z \sim 0.5$ to the similarly selected Las Campanas/AAT Rich Cluster Survey (LARCS) sample at $z \sim 0.1$, we find that the rest-frame $\delta(U - V)/\delta V$ slope of the colour–magnitude relation evolves with redshift which we attribute to the build up of the red sequence over time. This rest-frame slope evolution is not adequately reproduced by that predicted from semi-analytic models based on the Millennium Simulation despite a prescription for the build up of the red sequence by in-falling galaxies, 'strangulation'. We observe no strong correlation between this slope and the cluster environment at a given redshift demonstrating that the observed evolution is not due to a secondary correlation. Also presented are near-infrared United Kingdom Infrared Telescope (UKIRT) Wide Field CAMera (WFCAM) observations of the LARCS clusters which confirm and improve on the result from Stott et al. (2007) finding that there has been a two-fold increase in faint $M_V > -20$ galaxies on the red sequence since $z = 0.5$ to a significance of 5σ.

Key words: galaxies: clusters: general – galaxies: elliptical and lenticular, cD – galaxies: evolution.

1 INTRODUCTION

Galaxy clusters are important laboratories for the study of galaxy formation and evolution as they contain a concentrated population of diverse galaxies in a relatively small volume. Early workers in the field found that if a colour–magnitude diagram is plotted for members of local clusters such as Virgo and Coma, the Elliptical/S0 galaxies were found to be confined to a prominent linear feature in colour space (Visvanathan & Sandage 1977). This feature is known as the red sequence and has a very small intrinsic scatter (typically $<$0.1 mag) which has been interpreted as evidence that the passive galaxies in clusters formed coevally at high redshift (Bower, Lucey & Ellis 1992).

The red sequence is observed to have a slope such that the faint galaxies are bluer than the bright cluster members. The origin of the slope has been controversial due to the age metallicity degeneracy for stellar populations. Worthey, Trager & Faber (1995) showed that the sequence of colours that comprise the slope can be equally well explained by a progressive decrease in either metallicity or stellar age. The slope is now thought to be due to a mass–metallicity relation along the red sequence as this degeneracy was broken by comparing colour–magnitude simulations to observations of distant clusters (Kodama & Arimoto 1997). The origin of the mass–metallicity relation is thought to be the heating of the interstellar medium (ISM) by supernovae which triggers the formation of a galactic wind when the thermal energy of the gas exceeds the binding energy. This wind ejects gas more efficiently in smaller galaxies due to their shallower potential wells, resulting in the trend of increased metallicity with mass which manifests itself as the massive metal-rich galaxies appearing progressively redder than their less massive counterparts (Carlberg 1984; Arimoto & Yoshii 1987). Within the hierarchical picture of galaxy evolution, red sequence galaxies form the mergers of star-forming disc galaxies with the largest ellipticals being the product of the merger of the largest disc systems and are thus the most metal rich (Kauffmann & Charlot 1998).

The observed frame colour–magnitude relations for clusters at similar redshifts are found to have comparable slopes which have been shown to change with redshift (Lopez-Cruz 1997; Gladders et al. 1998; Lopez-Cruz, Barkhouse & Yee 2004). One explanation for this change in the observed slope is that it is a result of *K*-correction and an evolution in the mass–metallicity relation in cluster ellipticals (Kodama & Arimoto 1997). The change of slope

⋆E-mail: jps@astro.livjm.ac.uk

with redshift has been used as a method to constrain cluster galaxy evolution, with comparisons of the observed slope evolution to models suggesting that the elliptical galaxies in cluster cores have been in place since at least $z = 2$ (Gladders et al. 1998). However, other studies of the rest-frame slope have found little or no evolution suggesting that *K*-correction is the dominant factor (Stanford, Eisenhardt & Dickinson 1998; Blakeslee et al. 2003; Mei et al. 2006). This non-evolution has been used as evidence to favour monolithic collapse over hierarchical methods of galaxy formation.

Current research on the build up of the red sequence suggests that there may indeed be an age contribution to the red sequence slope and its evolution as faint, sub-L∗ galaxies, thought to have undergone recent star formation, are found to be transforming on to the sequence over time as they fall into the dense cluster environment (De Lucia et al. 2007; Stott et al. 2007; Smith et al. 2008). This is thought to be connected to the observation that there is a greater abundance of S0 galaxies in local clusters compared to their high-redshift counterparts, whose progenitors may be the quenched star-forming galaxies in higher redshift systems (Dressler et al. 1997; Smail et al. 1998). If this transformation scenario is correct then we expect to see evidence for it in the evolution of the rest-frame colour–magnitude relation.

Regardless of its origin, empirical observations and models of the colour and slope of the observed red sequence can be used in combination as a template to predict the redshift of a cluster. This is found to be in good agreement with spectroscopic redshifts and can therefore be used as an effective two-waveband photometric redshift. This technique is important for current and future large area photometric surveys which hope to study cluster abundance [e.g. Red Sequence Cluster Survey (RCS), Gladders & Yee 2000; Panoramic Survey Telescope & Rapid Response System (Pan-STARSS); Sloan Digital Sky Survey (SDSS), Adelman-McCarthy et al. 2006; UKIDSS, Lawrence et al. 2007; Swinbank et al. 2007].

In this work, we will investigate the red sequence slope evolution in observed optical [$\delta(V - I)/\delta I$] and near-infrared [$\delta(J - K)/\delta K$] bands and rest-frame optical [$\delta(U - V)/\delta V$] for a homogeneous sample of X-ray selected galaxy clusters in the range $z \sim 0$–1. This is the most comprehensive study of the red sequence slope undertaken thus far. We compare our findings with latest synthetic slopes calculated from analysis of the semi-analytical model of Bower et al. (2006) based on the Millennium *N*-body simulation (Springel et al. 2005). This model includes feedback from active galactic nuclei (AGN) which quenches star formation in massive haloes to match the observed break in the luminosity function seen at bright magnitudes. Another important process in this model is 'strangulation' which describes the stripping of a galaxy's hot-gas halo as it falls into a cluster leading to a cessation in star formation in lower mass galaxies thus providing a mechanism for the build up of passive red galaxies in the cluster (Larson, Tinsley & Caldwell 1980).

Λ cold dark matter (ΛCDM) cosmology ($\Omega_{\rm M} = 0.3$, $\Omega_{\rm Vac} = 0.7$, $H_0 = 70$ km s^{-1} Mpc^{-1}) is used throughout this work.

2 OBSERVATIONS AND REDUCTION

2.1 Cluster sample

To observe the evolution of the red sequence, we study X-ray selected clusters in the range $z = 0$–1 in both near-infrared and optical bands (Table 1). This is a large sample of the most X-ray luminous clusters known ($L_X > 10^{44}$ erg s^{-1}, 0.1–2.4 keV) which, with the exception of a handful of additional archival clusters, are all sourced from the *ROentgen SATellite* (*ROSAT*) All Sky Survey, although belong to the various subsamples named below. Such massive clusters are ideal for this study as their colour–magnitude relations are well populated. The motivation for studying an X-ray selected sample of clusters is to ensure that we are observing objects in similar high mass, high-density environments. This homogeneity is key to our study as we wish to compare clusters over a range of redshifts.

The main cluster samples studied in this paper, the MAssive Cluster Survey (MACS; Ebeling, Edge & Henry 2001; Ebeling et al. 2007) and the Las Campanas/AAT Rich Cluster Survey (LARCS; Pimbblet et al. 2001, 2006) are sufficiently X-ray luminous that they should correspond to the most extreme environments at their respective epochs. The median X-ray luminosities of the high and low redshift samples are 16.1 and 7.4 $\times$ 10^{44} erg s^{-1}, respectively, corresponding to a difference of less than a factor of 2 in the typical total mass (Popesso et al. 2005). However, an important issue to address is that the mass of the $z \sim 0.5$ progenitors of the LARCS clusters may be even lower than the MACS clusters. If we include the growth in halo mass through *N*-body mergers from Bower et al. (2006), we see that the progenitors of the LARCS clusters at $z \sim 0.5$ could be up to 3 times less massive than the MACS sample (with corresponding X-ray luminosities of 2 $\times$ 10^{44} erg s^{-1}, Popesso et al. 2005). There is no evidence for strong variations in the galaxy luminosity function between clusters spanning such a relatively modest difference in typical mass (de Propris et al. 1999). We therefore expect that any differences between the galaxy populations in these two samples will primarily reflect evolutionary differences between $z \sim 0.5$ and 0.1.

The 25 clusters observed in V and I or B and R bands belong to the following surveys: MACS (V_{F555W} and V_{F814W}, Cycle 12 GO project 9722); LARCS (B and R) and archival *Hubble Space Telescope* (*HST*) data ($V_{F555W/F606W}$ and V_{F814W}). The observations were taken with the instruments: the Advanced Camera for Surveys (ACS) and the Wide Field Planetary Camera (WFPC) on *HST* and the 1m Swope telescope at Las Campanas Observatory. For a more detailed description of the data and reduction see Stott et al. (2007) (MACS) and Pimbblet et al. (2001) (LARCS).

The 35 clusters studied in the near-infrared (J and K band) belong to: The MACS survey (Ebeling et al. 2001), the LARCS survey (Pimbblet et al. 2001), the *ROSAT* Brightest Cluster Survey (BCS) and extended BCS (Ebeling et al. 2000) and the X-ray Brightest Abell Clusters Survey (XBACS; Ebeling et al. 1996). The observations were taken with: the Wide field InfraRed Camera (WIRC) instrument on the Palomar 200 arcsec Hale telescope the Infrared Spectrometer And Array Camera (ISAAC) on the Very Large Telescope (VLT) and the Wide Field CAMera (WFCAM) on United Kingdom Infrared Telescope (UKIRT). An additional low-redshift data point is included for the Coma Cluster which we sourced from a combination of the Two Micron All Sky Survey (2MASS) extended and point source catalogues (Skrutskie et al. 2006). We refer the reader to Stott et al. (2008) for a more detailed description of the data and their reduction.

We include a high-redshift cluster (ClJ1226.9+3332, $z \sim 0.9$) from the Wide Angle *ROSAT* Pointed Surveys (WARPS; Scharf et al. 1997; Jones et al. 1998). This X-ray selected cluster was observed in the J and K bands using the UKIRT Fast-Track Imager (UFTI) camera on UKIRT (Ellis & Jones 2004).

2.2 Photometry

The colour ($V - I$, $B - R$ and $J - K$) photometry extracted for the cluster members employs 9 kpc diameter apertures for colours

Table 1. Details of the cluster sample used in our analysis which, with the exception of a handful of additional clusters, belong to *ROSAT* All Sky Survey. The LARCS and MACS redshifts are from Pimbblet et al. (2006) and Ebeling et al. (2007), respectively. $\kappa_{\rm opt.}$ and κ_{JK} are the observed optical and near-infrared slopes.

Cluster	RA	Dec.	z	L_X	$\kappa_{\rm opt.}$	κ_{JK}
	(J2000)			(10^{44} erg s^{-1})		
LARCS $z \sim 0.1$ Sample						
Abell 22	00 20 38.64	−25 43 19	0.142	5.3	-0.072 ± 0.014	-0.023 ± 0.010
Abell 550	05 52 51.84	−21 03 54	0.099	7.1	-0.055 ± 0.013	-0.024 ± 0.011
Abell 1084	10 44 30.72	−07 05 02	0.132	7.4	-0.058 ± 0.013	-0.033 ± 0.007
Abell 1285	11 30 20.64	−14 34 30	0.106	5.45	-0.036 ± 0.020	...
Abell 1437	12 00 25.44	+03 21 04	0.134	7.7	-0.037 ± 0.017	-0.010 ± 0.009
Abell 1650	12 58 41.76	−01 45 22	0.084	7.8	-0.047 ± 0.011	-0.019 ± 0.009
Abell 1651	12 59 24.00	−04 11 20	0.085	8.3	-0.048 ± 0.009	-0.002 ± 0.007
Abell 1664	13 03 44.16	−24 15 22	0.128	5.34	-0.054 ± 0.011	-0.021 ± 0.010
Abell 2055	15 18 41.28	+06 12 40	0.102	4.8	-0.066 ± 0.011	-0.021 ± 0.009
Abell 3888	22 34 32.88	−37 43 59	0.153	14.5	-0.047 ± 0.022	...
MACS $z = 0.4$–0.7 Sample						
MACS J0018.5+1626	00 18 33.68	+16 26 15	0.541	18.74	...	-0.048 ± 0.009
MACS J0025.4−1222	00 25 15.84	−12 19 44	0.478	12.4	-0.106 ± 0.021	-0.047 ± 0.010
MACS J0257.6−2209	02 57 07.96	−23 26 08	0.504	15.4	-0.105 ± 0.014	-0.065 ± 0.012
MACS J0454.1−0300	04 54 11.13	−03 00 53.8	0.550	16.86	...	-0.040 ± 0.013
MACS J0647.7+7015	06 47 51.45	+70 15 04	0.584	21.7	-0.090 ± 0.024	...
MACS J0712.3+5931	07 12 20.45	+59 32 20	0.328	6.8	-0.044 ± 0.006	...
MACS J0717.5+3745	07 17 31.83	+37 45 05	0.548	27.4	-0.068 ± 0.012	...
MACS J0744.8+3927	07 44 51.98	+39 27 35	0.686	25.9	-0.081 ± 0.023	...
MACS J0911.2+1746	09 11 10.23	+17 46 38	0.506	13.2	-0.087 ± 0.011	...
MACS J1149.5+2223	11 49 34.81	+22 24 13	0.544	17.3	-0.101 ± 0.011	...
MACS J1354.6+7715	13 54 19.71	+77 15 26	0.397	8.2	-0.057 ± 0.018	...
MACS J1359.8+6231	13 59 54.32	+62 30 36.3	0.330	8.83	...	-0.039 ± 0.007
MACS J1423.8+2404	14 23 47.95	+24 04 59	0.544	15.0	-0.078 ± 0.013	...
MACS J2129.4−0741	21 29 25.38	−07 41 26	0.570	16.4	-0.115 ± 0.017	-0.068 ± 0.009
MACS J2214.9−1359	22 14 56.51	−14 00 17	0.495	17.0	-0.100 ± 0.012	-0.035 ± 0.014
Additional *ROSAT* All Sky Survey clusters						
Abell 115	00 56 00.24	+26 20 31.7	0.197	14.59	...	-0.031 ± 0.006
Abell 209	01 31 52.51	−13 36 41.0	0.209	13.75	...	-0.022 ± 0.009
Abell 291	02 01 46.80	−02 11 56.9	0.196	4.24	...	-0.024 ± 0.009
Abell 665	08 30 57.34	+65 50 31.4	0.182	16.33	...	-0.020 ± 0.008
Abell 773	09 17 53.57	+51 44 02.5	0.217	13.08	...	-0.033 ± 0.006
Abell 1201	11 12 54.50	+13 26 08.9	0.169	6.28	...	-0.013 ± 0.007
Abell 1246	11 23 58.75	+21 28 47.3	0.190	7.62	...	-0.031 ± 0.008
Abell 1703	13 15 00.70	+51 49 10	0.258	8.7	-0.057 ± 0.012	...
Abell 1758	13 32 38.59	+50 33 38.7	0.279	11.68	...	-0.027 ± 0.011
Abell 1763	13 35 20.14	+41 00 03.8	0.223	14.93	...	-0.029 ± 0.010
Abell 1914	14 25 56.64	+37 48 59.4	0.171	18.39	...	-0.021 ± 0.006
Abell 2111	15 39 41.81	+34 24 43.3	0.229	10.94	...	-0.033 ± 0.012
Abell 2163	16 15 33.57	−06 09 16.8	0.203	37.50	...	-0.022 ± 0.006
Abell 2218	16 35 49.39	+66 12 45.1	0.176	9.30	...	-0.025 ± 0.007
Abell 2445	22 26 55.80	+25 50 09.4	0.165	4.00	...	-0.027 ± 0.009
RX J1720.1+2638	17 20 10.08	+26 37 33.5	0.164	6.66	...	-0.023 ± 0.007
Zw 1432	07 51 25.15	+17 30 51.8	0.186	5.27	...	-0.022 ± 0.010
Additional archival clusters						
Cl J0152−1357	01 52 43.91	−13 57 21	0.831	5.0	-0.084 ± 0.026	...
Cl J1226.9+3332	12 26 58.13	+33 32 49	0.890	20.0	-0.088 ± 0.016	-0.088 ± 0.010
Coma Cluster	12 59 48.70	+27 58 50.0	0.0231	7.26	-0.075 ± 0.015	-0.017 ± 0.009
MS1054−0321	10 57 00.20	−03 37 27.4	0.830	23.30	...	-0.073 ± 0.011
RCS0224−0002	02 24 00.00	−0 02 00.0	0.770	0.70	...	-0.055 ± 0.020

and the magnitude used is SEXTRACTOR's 'best' magnitude (Bertin & Arnouts 1996). This choice of aperture is significantly greater than the seeing conditions in which the low redshift ground-based optical and near-infrared data were taken, typically ∼1.0–1.2 arcsec, giving LARCS sample photometric apertures of ∼4 arcsec whereas the higher redshift MACS sample is extracted with ∼1.4 arcsec apertures, considerably larger than the *HST* ACS point spread function. We are therefore confident that we are collecting a comparable fraction of light for galaxies at different redshifts. We observe no trend between colour and seeing for our LARCS low-redshift optical data,

although the seeing is consistent, and as the high-redshift sample is observed with *HST* this is not a concern. We also investigate this for the $z \sim 0.1$–0.3 clusters observed in the near-infrared wavebands for which colour is again independent of seeing, even though the conditions are more variable for our additional *ROSAT* clusters sample (0.9–1.5 arcsec).

The SEXTRACTOR colour photometry was run in dual mode, on point spread function matched images using the IRAF PSFMATCH package, with the 9 kpc 'red'-band (R, I, K) apertures used to extract the corresponding 'blue'-band (B, V, J) photometry. This is to ensure the same size aperture for both bands which is important for good colour determination. Star and Galaxy separation is performed using SEXTRACTOR where detected objects with CLASS_STAR < 0.1 and/or $J - K > 0.95$ (for the near-infrared sample) are classified as galaxies with the stars removed from the analysis. We only consider galaxies within 600 kpc radius of the cluster centre, to limit contamination from field galaxies. All of our observations reach a depth which allows us to see to at least 4 mag fainter than the Brightest Cluster Galaxy (BCG) and thus perform a reliable fit to the slope and probe the sub-L* galaxy population where the red sequence build up is taking place.

A potential problem with all aperture photometry is that the galaxies themselves may have significant internal colour gradients thought to be associated with a metallicity gradient between the outer and inner parts of the system. As stated above, we are observing the same fraction of light from galaxies at all redshifts which should limit this effect unless there is a significant evolution in the colour gradient of galaxies with redshift, although this would be an interesting effect in itself. Studies of the internal colour gradients of moderate redshift cluster galaxies using high-quality *HST* data have found no such evolution in mean colour gradient and redshift, with the individual cluster galaxies appearing to have random colour gradients Tamura & Ohta (2000). We therefore conclude that any variations in internal colour gradient would act randomly to make galaxies appear either redder or bluer resulting in increased scatter of the red sequence but not an evolution in its slope.

2.3 WFCAM data

We obtained near-infrared J- and K-band data for eight of the LARCS $z \sim 0.1$ clusters with WFCAM on UKIRT. WFCAM consists of four detectors in a square, each separated by a gap comparable in size to a single detector, with a central autoguider. Each detector is a Rockwell Hawaii II 2048 × 2048 PACE HgCdTe array, with pixel size 0.4 arcsec. WFCAM single pointings or 'footprints' do not observe a contiguous area of sky so to create a mosaiced image four of these WFCAM footprints are tiled to make a 4 × 4 detector image. In addition to this tiling, the WFCAM images incorporate 'microstepping' which is a small dither pattern in the observation. The purpose of this process is to improve the point spread function sampling of the observations as the 0.4 arcsec pixel size of WFCAM is comparable to the best atmospheric seeing. The microstepping is performed by observing four images each offset from each other by a whole number of pixels and a 1/2 pixel in a 2 × 2 grid pattern. These images are then co-added together with the fractional offsets taken into account so that the resulting image has double the spatial sampling. Therefore, a detector image with an original resolution of 0.4 arcsec pixel^{-1} and size 2048 × 2048 pixel are converted to a higher resolution 0.2 arcsec pixel^{-1} 4096 × 4096 image.

The observations took place during service mode on the nights of 2006 December 5 and 2007 April 19 in 1.0 and 1.2 arcsec seeing conditions, respectively. The total integration times for the J- and K-band images are 200s each, composed of 10s exposures in a five point dither pattern with 2 × 2 microstepping. To create a contiguous Mosaic of WFCAM images, we run the TERAPIX SWARP software on the data which gives an image with a world coordinate system consistent to within 0.1 arcsec of the 2MASS and the United States Naval Observatory (USNO) star catalogue across the whole field of view. To extract the J- and K-band catalogues from the mosaiced images, we use the SEXTRACTOR software in dual mode so that the K-band catalogue detections are used to extract the J-band photometry in an identical process to above. The photometry is calibrated using the 2MASS point source catalogue and we find the J and K band 5σ vega limits of these data are 19.50 and 17.75 mag, respectively.

2.3.1 *Quantifying the dwarf to giant ratio of the LARCS clusters*

The WFCAM instrument allows us to create contiguous images that are ∼0.9 on the side which corresponds to 5.6 Mpc at $z = 0.1$. With images of this size, we can study both the cluster and the surrounding field galaxy population. A number of recent papers have studied the form of the colour–magnitude relation in galaxy clusters with some reporting a dearth of faint red sequence galaxies at high redshift (e.g. De Lucia et al. 2004, 2007; Kodama et al. 2004). Stott et al. (2007) demonstrate that faint red galaxy population in clusters is built up over time by analysing the ratio of faint to luminous galaxies along the red sequence in a homogenous sample of clusters at $z \sim 0.1$ and 0.5. One of the limiting factors in that study was the uncertainty in the faint end statistical field correction for the LARCS $z \sim 0.1$ colour–magnitude relations. However, the uncertainty in the field correction is reduced if near-infrared observations are employed as it is easier to isolate the cluster red sequence. A comparison of Fig. 1 with the equivalent optical colour magnitude diagram, Fig. 1 (bottom right panel), of Stott et al. (2007) illustrates this point.

By analysing the WFCAM data in an identical way to that described in Stott et al. (2007) in concert with the UKIDSS Deep eXtragalactic Survey (DXS, Survey Head: Alastair Edge) field observations we can successfully quantify both the cluster and field galaxy population. The field correction is performed by dividing the colour–magnitude space of the cluster and field samples into a two-dimensional histogram and subtracting the field number counts from the cluster population (Stott et al. 2007). The Poisson errors from this field correction are folded through into the final result. To determine the relative numbers of faint and luminous galaxies on the red sequence, we define the red sequence dwarf to giant ratio (RDGR). This quantity is defined as the number of dwarf (faint) galaxies divided by the number of giant (luminous) galaxies on the cluster red sequence after the statistical subtraction of the field

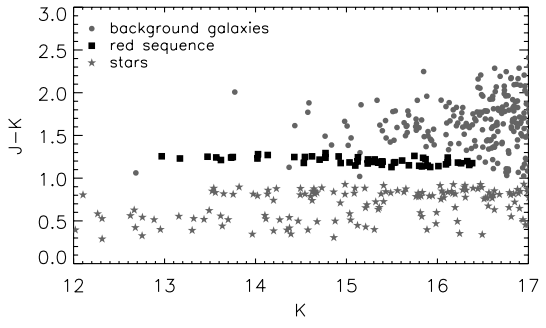

Figure 1. The $(J - K)$ versus K colour–magnitude diagram for the cluster Abell 1084 which demonstrates the ease at which near-infrared colours separate the red sequence from stellar and field galaxy contamination.

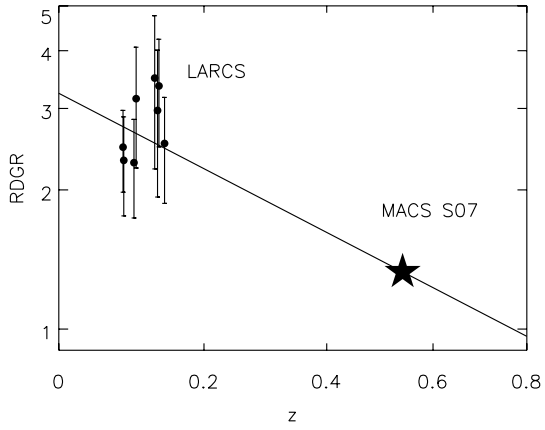

Figure 2. The evolution of the RDGR with redshift comparing the MACS sample from Stott et al. (2007) with the LARCS WFCAM sample. A fit of the form $(1 + z)^{-\beta}$ to the LARCS and MACS samples is plotted which yields $\beta = -2.1 \pm 0.3$.

galaxy population. The dividing line between dwarfs and giants, for consistency with the Stott et al. (2007) result, is given in absolute V-band magnitude, $M_V = -19.9$ and a limiting magnitude of $M_V = -17.75$ for the faintest dwarfs, a correction for passive evolution is applied when studying high-redshift samples. We convert these limits to apparent K-band magnitudes, $K \sim 14.7$ and $\sim$16.8, respectively (depending on the precise redshift), using a Bruzual & Charlot (2003) simple stellar population with solar metallicity and a formation redshift, $z_f = 5$.

The weighted mean of the RDGRs of the eight LARCS clusters from this sample is 2.59 ± 0.24 compared to the Stott et al. (2007) result of 2.93 ± 0.45. We can now say that when compared to our $z \sim 0.5$ MACS sample, where the DGR $= 1.33 \pm 0.06$, the ratio of dwarf to giant galaxies on the cluster red sequence has increased by a factor of 1.95 ± 0.20 in the past 5 Gyr which confirms and improves the significance of the result of Stott et al. (2007) from 3σ to 5σ. This is strong evidence for a significant build up of the red sequence in massive clusters. Fig. 2 is the equivalent of fig. 2 (right-hand side) of Stott et al. (2007) and displays the evolution in the RDGR with redshift for rich galaxy clusters. To parametrize this evolution, we fit a $(1 + z)^{-\beta}$ power law to the LARCS and MACS samples where $\beta = -2.1 \pm 0.3$ with all clusters consistent with the fit.

3 ANALYSIS AND RESULTS

3.1 Fitting red sequence the slope

Figs 3 and 4 are examples of the prominent red sequences we see in the rich clusters of our sample. To fit the slope of the red sequence, we need to use a robust and consistent method. We therefore employ the same technique as described in Gladders et al. (1998), an iterated 3σ clipped fit. The fit is performed as follows: first, we set a limiting magnitude for the red sequence which corresponds to the mean of the next two brightest galaxies down from the BCG magnitude+3. The reason for this is that in some cases there can be a large luminosity gap ($\sim$1 mag) between the BCG and the start of the red sequence so this ensures that we measure the slope without this gap. The fit is performed over 3 mag to incorporate the sub-L* galaxy population which show the strongest evidence for red sequence build up (Stott et al. 2007). We select the region of colour–magnitude space containing the red sequence and estimate an initial fit from visual inspection. The residuals about this estimate are calculated and a Gaussian is fitted to the resulting colour distribution with the slope removed. The peak of this Gaussian corresponds to the red sequence. We then perform a fit to points that are within 3σ of this fit. This is a two parameter linear fit of the form $y = \kappa x + c$ where κ is the slope of the red sequence. The process is iterated until it converges to a solution. We confirm the work of Gladders et al. (1998) that this is a robust method for reasonable choices of limiting magnitude and initial fit.

It should be noted that our colour–magnitude diagrams are not field corrected as the rich clusters in our sample have well-populated red sequences in contrast to the field. At the colours and magnitudes, we consider this a very small contribution to the red sequence, typically 5 per cent contamination for the MACS clusters and 10 per cent for the LARCS clusters. We perform a statistical field correction test to a subsample of our low-z clusters and find that the slope of the sequence varies randomly by less than 1σ than that obtained for the uncorrected sequence. We therefore feel justified in not applying this correction. For details of the statistical field correction technique used see Stott et al. (2007).

3.2 Model slope evolution

We form a prediction of how the red sequence slope evolves, by analysing the semi-analytical model of Bower et al. (2006) based on the Millennium N-body simulation (Springel et al. 2005). We access these data on-line through Virgo Millennium Data base. The Bower et al. (2006) model accounts for the recent observations that the stellar mass in bright galaxies was in place at high redshift by including feedback from AGN. It also includes a prescription for the build of the red sequence via 'strangulation'. This describes a process whereby galaxies falling into a cluster are stripped of their hot gas reservoir upon interaction with the intracluster medium quenching star formation (Larson et al. 1980).

We define model clusters as dark matter haloes above a threshold mass which contain bound subhaloes (galaxies) with observational properties assigned to them by semi-analytic modelling. To allow comparison between models and observation, we assume that the model cluster members are analogous to the red sequences of our observed clusters. We need to select clusters from Bower et al. (2006) which are comparable in mass to those we observe. By using the relation between cluster mass and X-ray luminosity (Popesso et al. 2005), we include only the simulated haloes with $M_{200} > 3.4 \times 10^{14}\,M_\odot$ which corresponds to $L_X > 10^{44}$ erg s^{-1}. To select only the most massive systems for comparison with our observations, we limit our red sequence fit to a stack of the top five ranked clusters by mass in each redshift bin. The model slope is robust to our choice of lower mass limit as we see no significant change in our slope values when using all haloes with masses greater than mean halo mass in the required redshift interval.

We model the red sequence slope evolution by creating stacked colour–magnitude diagrams from the Bower et al. (2006) model output at a distinct set of redshift intervals between $z = 0$ and 1. For the creation of these colour–magnitude diagrams, we ensure that we only study the passive red sequence galaxies by selecting galaxies with no current star formation [$L(\mathrm{H}\alpha) = 0$]. The models provide no spatial information but we assume that the synthetic colours we calculate from the total magnitudes can be compared with the observed aperture magnitudes allowing for a normalization between the model and observed slope evolution at low redshift.

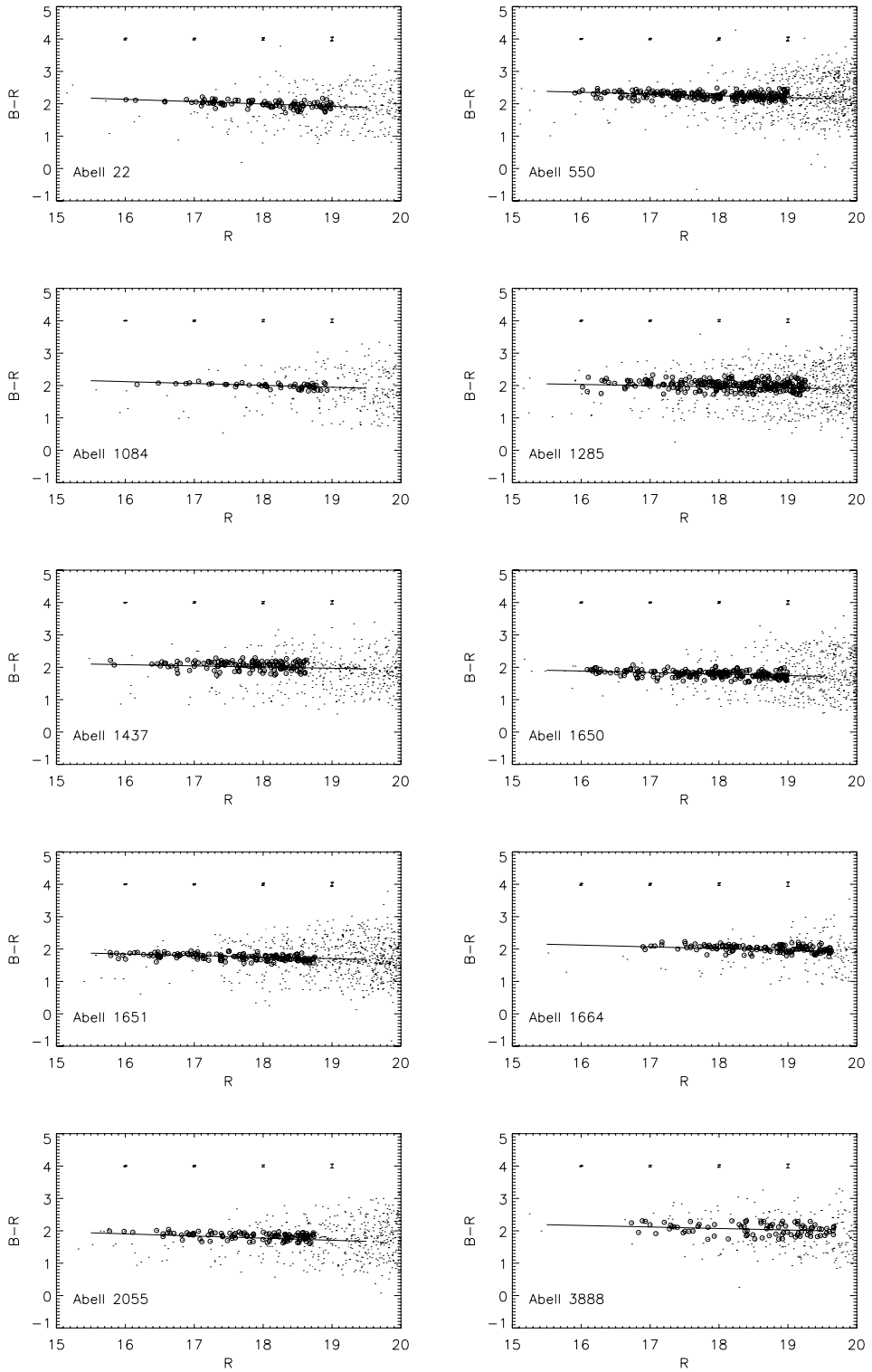

Figure 3. The LARCS optical colour–magnitude diagrams with the red sequence fits overplotted. Representative error bars are shown for a range of magnitudes.

We calculate the model for the observed frame slope evolution and its errors by fitting to the stacked synthetic red sequence slopes at each redshift interval with the method described in Section 3.1. As with the observations, the model slope is shown to steepen with redshift.

3.3 Observed slope evolution

Fig. 5 displays the observed red sequence slope evolution for our near-infrared sample. The slope $[\kappa_{JK} = \delta(J - K)/\delta K]$ is shown to steepen with redshift. This steepening will have contributions from both K-correction and perhaps an age or a metallicity evolution. The

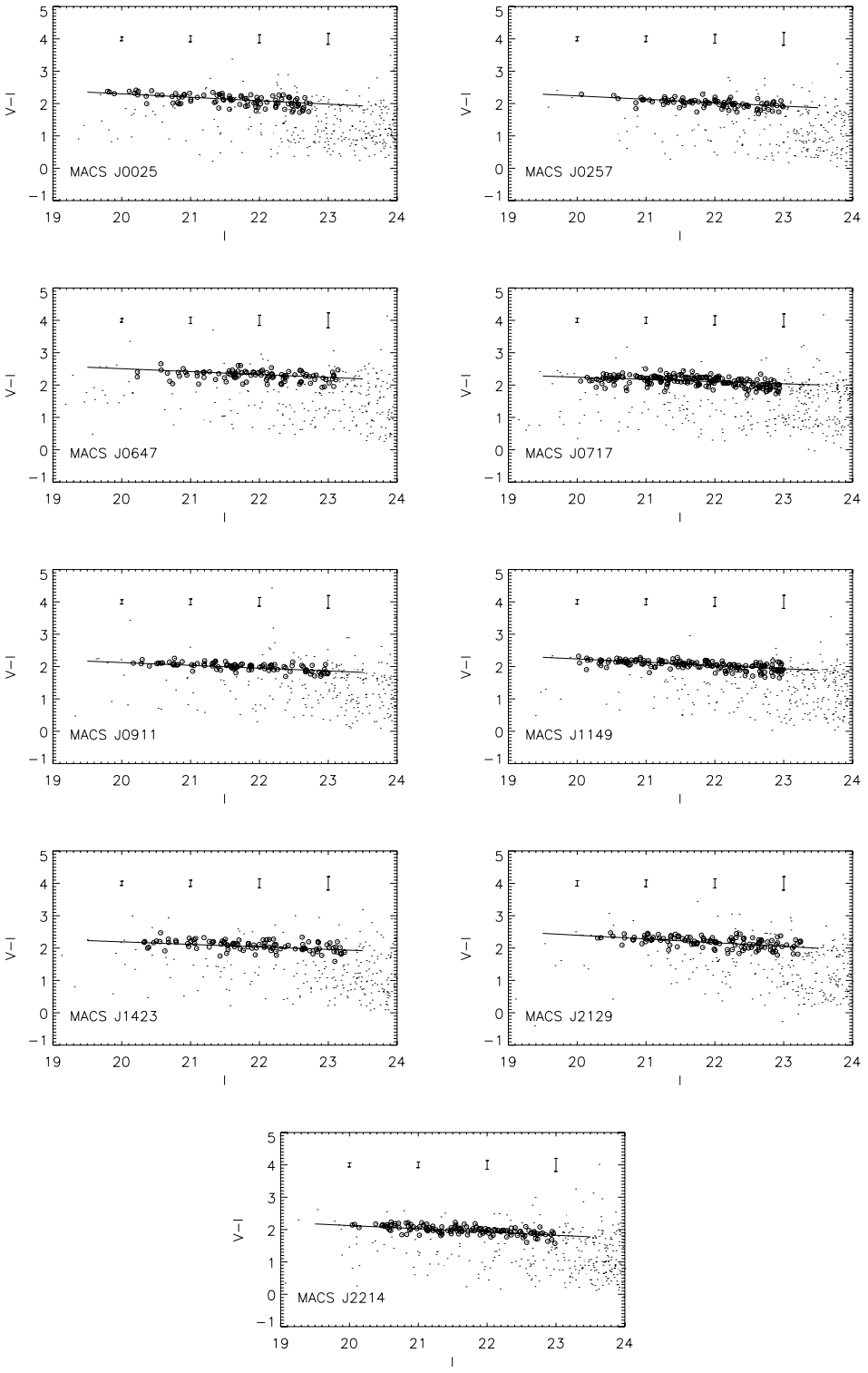

Figure 4. The main MACS sample optical colour–magnitude diagrams with the red sequence fits overplotted. Representative error bars are shown for a range of magnitudes.

contribution from *K*-correction is due to the observed *J* and *K* bands sampling increasingly bluer rest wavebands at higher redshift which affects galaxies differentially along the red sequence depending on their spectral energy distributions (Gladders et al. 1998; Pimbblet et al. 2001).

When the model described in Section 3.2 is plotted with our complete near-infrared data set in Fig. 5, we find good quantitative agreement between the two with the data having an rms scatter about the model of 0.009 which is comparable to the calculated error on the model (mean 1σ error is 0.006).

We now investigate the slope $[\kappa_{VI} = \delta(V-I)/\delta I]$ evolution for our optical observations. As above, the simulated slope evolution plotted is calculated from semi-analytical model of Bower et al. (2006). There is an additional complication as our optical data are

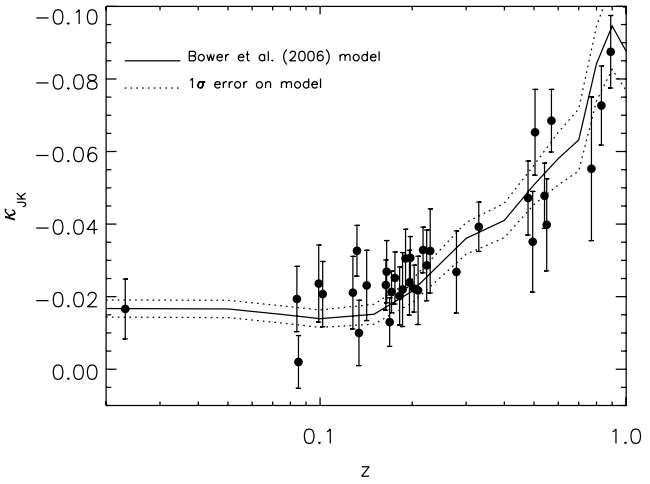

Figure 5. The evolution of the red sequence slope (κ_{JK}) for our near-infrared sample. A model calculated from Bower et al. (2006) is included for comparison with theory.

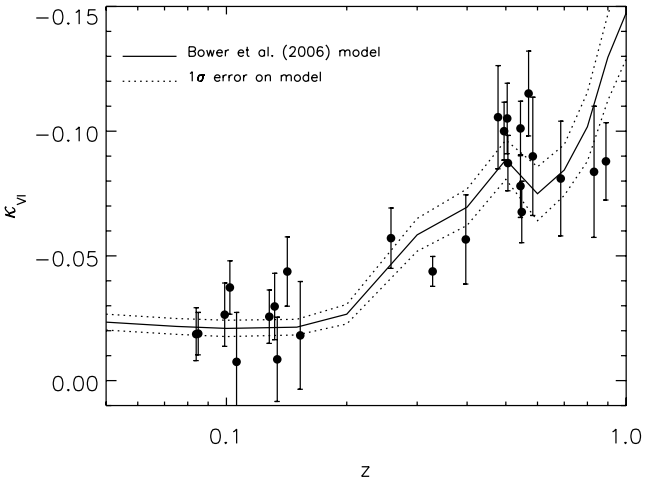

Figure 6. The evolution of the red sequence slope (κ_{VI}) for our optical sample. The model again comes from analysis of Bower et al. (2006).

sourced from two different filter sets so we have to account for the observed difference in red sequence slope between them. To achieve this, we normalize all data to the $\delta(V-I)/\delta I$ filters by correcting for the difference between the $\delta(V-I)/\delta I$ model and the model for the $\delta(B-R)/\delta R$ filter combination (as in Gladders et al. 1998). The resultant data-points and model are plotted in Fig. 6. The slope is shown to increase with redshift as above. The rms scatter about the model is 0.017 (compared to the mean 1σ error in the model of 0.008) so as with the near-infrared observations we find good agreement between the model and the data.

3.3.1 Rest-frame slope evolution

To investigate the intrinsic evolution of the red sequence slope we need to study clusters observed with matched rest-frame photometry. This is to quantify the proposed contribution from the build up of the red sequence without the additional effect of *K*-correction. We can observe this intrinsic slope evolution as our two main sets optical observations, the $z\sim0.1$ LARCS clusters in $(B-R)$ colour and the $z\sim0.5$ MACS clusters in $(V-I)$ colour, both correspond

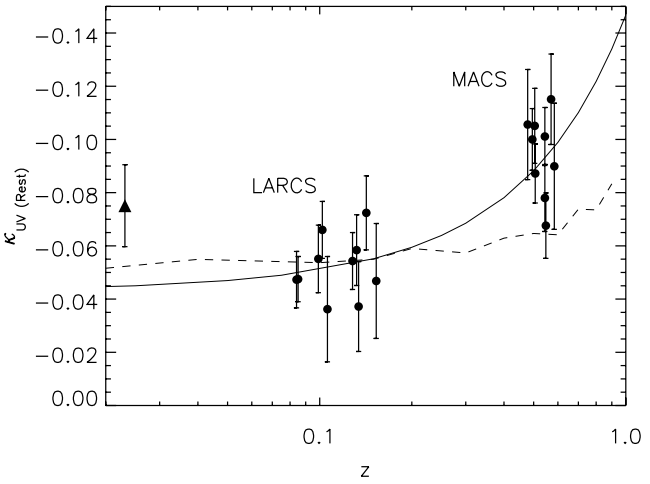

Figure 7. The evolution of the rest-frame red sequence slope (κ_{UV}) for our optical sample. The triangle is the data point for the Coma Cluster. The solid line is a fit to the MACS and LARCS data of the form $(1+z)^{\beta}$ where $\beta=1.77\pm0.25$. The dashed line is the rest-frame slope evolution calculated from the semi-analytic model of Bower et al. (2006).

to the rest-frame $(U-V)$ colour at their respective epochs. $(U-V)$ colour straddles the 4000 Å break and therefore is a good discriminant between the red sequence and star-forming cluster members/foreground galaxies. We confirm that the filters are well matched to rest-frame $(U-V)$ as we find a colour term of 1.0 ± 0.05 between the $B-R$ at $z=0.11$ and $V-I$ at $z=0.53$ using the technique described in Blakeslee et al. (2006).

The evolution of this intrinsic slope [$\kappa_{UV}=\delta(U-V)/\delta V$] is plotted in Fig. 7. We include an additional low redshift data-point for the Coma cluster calculated from the Sloan Digital Sky Survey (SDSS; Adelman-McCarthy et al. 2006) *u* and *g* filter photometry. In this figure, we can see that the intrinsic optical slope, κ_{UV}, does evolve with redshift as the intermediate *z* MACS clusters have a steeper red sequence than their low *z* LARCS counterparts. The weighted mean values for the LARCS and MACS κ_{UV} are -0.053 ± 0.004 (s.e.m) and -0.092 ± 0.004 standard error of the mean (s.e.m) respectively, a difference of 6.5σ. We can therefore say that there is a real contribution to the slope evolution from factors other than *K*-correction. The fit to the data in Fig. 7 is of the form $(1+z)^{\beta}$ where $\beta=1.77\pm0.25$. We note that the Coma Cluster has a steeper slope than the rest of our low redshift sample, although only a $\sim2\sigma$ discrepancy from the fit, which we may expect as it is found to have lower than average dwarf-to-giant ratio along its red sequence suggesting it is still undergoing faint end and therefore slope evolution (Stott et al. 2007). Including the Coma Cluster does not have a significant affect on the fit, $\beta=1.67\pm0.26$.

The dashed line plotted on Fig. 7 is the rest-frame $\kappa_{UV}=\delta(U-V)/\delta V$ slope calculated from the semi-analytic model of Bower et al. (2006), normalized to the mean value of the LARCS sample slope, which shows only a mild evolution with redshift and is therefore unable to replicate the rest-frame slope change observed. From this we can conclude that the major contribution to the agreement between the observed slope evolution in Section 3.3 and that derived from the semi-analytic modelling shown in Figs 5 and 6 was the *K*-correction differential between high and low mass galaxies along the synthetic red sequence and that a significant, intrinsic, slope evolution is not predicted by the models.

3.4 Evolution with other observables

We now investigate whether there are further trends in red sequence slope with other observable cluster properties to ensure that the result seen in Section 3.3.1 is not due to a secondary correlation. The most obvious of these being the X-ray luminosity, which is a proxy for mass in a relaxed system. In Figs 8 and 9, we plot the residual values of the slope about the model line in Fig. 5 and fit in Fig. 7 against L_X. From this we see no significant trend between scatter about the model and L_X as the Pearson correlation coefficients, r, for the near-infrared and optical data are 0.17 and 0.24 respectively which is actually a weak anticorrelation between steepening negative red sequence slope and L_X. However, because of the magnitude of the errors on both the individual slope measurements and the models, we need to quantify what level of trend the errors could accommodate before becoming observable. For the near-infrared sample, we find that a steepening greater than 0.010 in the slope in $L_X = 26.6 \times 10^{44}$ erg s^{-1} can be ruled out with a 3 sigma confidence whereas for the rest-frame $(U - V)$ sample we find this magnitude of change can occur in $L_X = 12.3 \times 10^{44}$ erg s^{-1}. The difference in mean L_X between the LARCS and MACS samples is 8.5×10^{44} erg s^{-1} for which we can rule out, with a 3 sigma confidence, increases in slope greater than 0.007, if we use the $(U - V)$ result, or 0.003 if we use the $J - K$ result. For the rest-frame $\delta(U - V)/\delta V$ slope evolution in Fig. 7, we see that the observed change in rest-frame slope of $\sim$0.04 cannot be accounted for by the difference in L_X alone and is, we believe, a definite trend with redshift. In Fig. 10, we also show that there is no significant trend between red sequence slope and another mass proxy, the cluster velocity dispersion, $\sigma (r = 0.27)$, which is again a weak anticorrelation. As above we can rule out increases in slope greater than 0.010 with 3σ confidence between the average velocity dispersions of the MACS and LARCS samples.

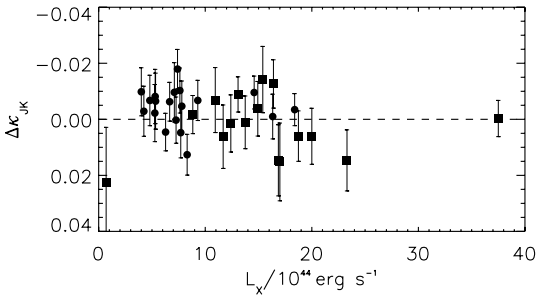

Figure 8. The residuals about the models in Fig. 5 plotted against X-ray luminosity. Filled circles and squares represent galaxy clusters with redshifts, $z < 0.2$ and >0.2 respectively, to demonstrate there is no redshift dependence. The correlation coefficient, r, for this plot is 0.17.

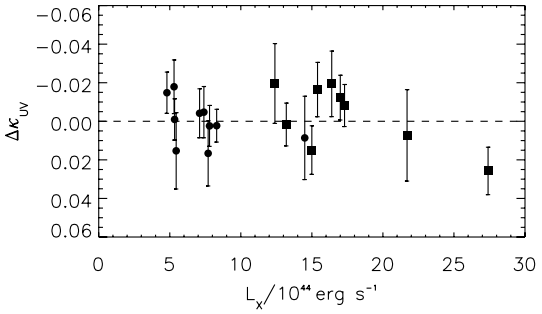

Figure 9. The residuals about the models in Fig. 7 plotted against X-ray luminosity. Filled circles and squares represent galaxy clusters with redshifts, $z < 0.2$ and >0.2, respectively, to demonstrate there is no redshift dependence. The correlation coefficient, r, for this plot is 0.24.

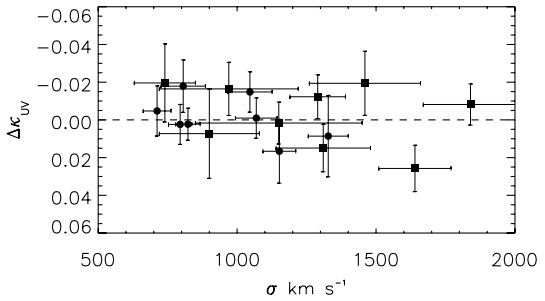

Figure 10. The residuals about the models in Fig. 7 plotted against velocity dispersion, σ. Filled circles and squares represent galaxy clusters with redshifts, $z < 0.2$ and >0.2, respectively, to demonstrate there is no redshift dependence. The MACS and LARCS cluster velocity dispersions are sourced from Ebeling et al. (2007) and Pimbblet et al. (2006), respectively. The correlation coefficient, r, for this plot is 0.27.

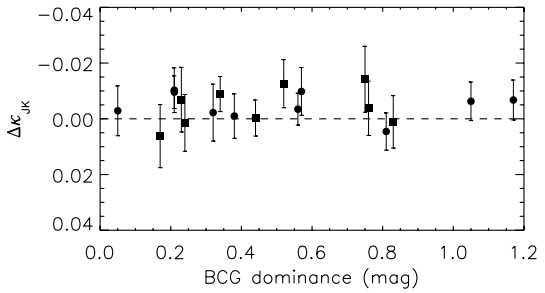

Figure 11. The residuals about the models in Fig. 5 plotted against BCG dominance. Filled circles and squares represent galaxy clusters with redshifts, $z < 0.2$ and >0.2, respectively, to demonstrate that there is no redshift dependence. The correlation coefficient, r, for this plot is -0.09.

In addition to the X-ray luminosity and σ, we can look to the degree of BCG dominance as an indicator of the local environment within the cluster core. This parametrizes the luminosity gap between the BCG and the next brightest galaxies on the red sequence and is defined as $\delta m_{1-2,3} = (m_2 + m_3)/2 - m_1$ where m_1 is the magnitude of the BCG and m_2 and m_3 are the magnitudes of the 2nd and 3rd brightest members respectively (Kim et al. 2002; Stott et al. 2008). The BCG may be the dominant elliptical in a cluster centre containing much smaller galaxies or it may be in a system were it is only marginally brighter than the next brightest members. In Fig. 11, we demonstrate that there is no strong trend between red sequence slope and the degree of BCG dominance ($r = -0.09$) and can rule out increases of slope greater than 0.01 in 0.61 mag of dominance with a 3 sigma confidence.

The above results suggest that different cluster environments do not have a strong effect on the near-infrared or optical red sequence slope at a given redshift, demonstrating that the result in Section 3.3 is robust. Previous studies within a similar L_X range have also seen homogeneity in other related cluster properties such as the shape of the luminosity function and the blue galaxy fraction (de Propris et al. 1999; Wake et al. 2005).

4 DISCUSSION

In this work, we have found a significant evolution in the rest-frame slope of the red sequence in rich galaxy clusters between $z \sim 0.5$ and $z \sim 0.1$. We propose that this intrinsic evolution is due to

galaxies falling into the cluster core and transforming on to the red sequence (De Lucia et al. 2007; Stott et al. 2007). If these galaxies have undergone recent star formation in filaments (e.g. Porter et al. 2008), which has been quenched by interactions as they fall into the cluster, they will appear bluer than other passive galaxies in the cluster due to their young age. These galaxies will redden more rapidly with time than their old, luminous counterparts flattening the red sequence at progressively lower redshift. This relates to the concept of downsizing which describes the observation that star formation ceases in the largest galaxies first so that it takes place mainly in lower mass galaxies at late times (Cowie et al. 1996).

An alternative or additional explanation is that this result is caused by a differential chemical evolution along the red sequence. A differential chemical evolution along the sequence which preferentially enriches the faint galaxies could lead to a steeper red sequence slope at high redshift. The supposition of a metallicity differential along the sequence that decreases with redshift is borne out in the semi-analytic models as the gradient at $z = 0$ is -0.0029 ± 0.0004 $Z_{\odot}$ mag^{-1} and at $z = 1$ it is -0.061 ± 0.009 $Z_{\odot}$ mag^{-1}. However, this may be non-physical with the primary goal of semi-analytic model is to match the observed properties of the local Universe and not necessarily the evolution from high redshift.

This result is in disagreement with the work of Stanford et al. (1998), Blakeslee et al. (2003) and Mei et al. (2006) who find no evidence for intrinsic slope evolution. There are several potential reasons for this disagreement. We first note the scatter in the values of the slope which could obscure the intrinsic evolution in previous studies without the coverage per redshift bin we have in our sample. This scatter is important when choosing a low redshift comparison cluster, some earlier works use a single cluster, usually Coma, which we have shown to have an unusually steep red sequence compared to the mean of our low z sample. The use of Coma would therefore tend to bias the result towards no evolution. The choice of $(U - B)$ rest-frame colour in previous studies means that they are observing a smaller dynamic range in colour than our $(U - V)$ sample. This is particularly important if the rest-frame '$U - B$' colours do not effectively straddle the 4000 Å break (e.g. fig. 4 of Mei et al. 2006) which may result in contamination of the red sequence by both foreground galaxies and star-forming cluster members. We also ensure that we perform all of the red sequence slope fits using the same homogenous method rather than importing slopes from other studies which may have a systematic offset.

The good agreement found between our data and slope evolution models calculated from semi-analytical model of Bower et al. (2006) in Figs 5 and 6 is mainly due to the treatment of *K*-correction rather than any significant slope evolution. This demonstrates that although such models include 'strangulation' of star-forming galaxies falling into cluster environments, they are unable to effectively reproduce the intrinsic evolution seen in our sample. This deficiency is also seen when studying the build up of the red sequence (Gilbank & Balogh 2008). We speculate that an improved prescription for a strangulation-like process in the semi-analytic models will be an important factor in recreating observations of an intrinsic slope evolution and build up of the red sequence.

When looking at slope trends with other observables we see no relationship between cluster slope and X-ray luminosity, velocity dispersion or BCG degree of dominance. This suggests that there is very little variation between the red sequence slopes due to the different cluster environments demonstrating that the main result of this paper is robust to the differing global properties within our sample. This implies that searching for massive clusters using the colour–magnitude relation, as employed by current and future large area optical/near-infrared surveys, is a viable method (e.g. RCS, Gladders & Yee 2000; Pan-STARSS; SDSS, Adelman-McCarthy et al. 2006; UKIDSS, Lawrence et al. 2007; Swinbank et al. 2007).

ACKNOWLEDGMENTS

We thank the referee for their useful comments which have improved the clarity and conclusions of this paper. Thanks also go to Richard Bower, Philip Best, Jim Geach and Matt Hilton for useful discussions. JPS acknowledges support through a Particle Physics and Astronomy Research Council and latterly a Science and Technology Facilities Council Studentship. KAP acknowledges partial support from the Australian Research Council and partial support from a University of Queensland ResTeach Fellowship.

The United Kingdom Infrared Telescope is operated by the Joint Astronomy Centre on behalf of the Science and Technology Facilities Council of the U.K. We gratefully acknowledge the allocation of UKIRT service time for our observations.

This publication makes use of data products from the 2MASS, which is a joint project of the University of Massachusetts and the Infrared Processing and Analysis Centre/California Institute of Technology, funded by the National Aeronautics and Space Administration and the National Science Foundation.

The Millennium Simulation data bases used in this paper and the web application providing online access to them were constructed as part of the activities of the German Astrophysical Virtual Observatory.

REFERENCES

Adelman-McCarthy J. K. et al., 2006, ApJS, 162, 38
Arimoto N., Yoshii Y., 1987, A&A, 173, 23
Bertin E., Arnouts S., 1996, A&AS, 117, 393
Blakeslee J. P. et al., 2003, ApJ, 596, 143
Blakeslee J. P. et al., 2006, ApJ, 644, 30
Bower R. G., Lucey J. R., Ellis R. S., 1992, MNRAS, 254, 589
Bower R. G., Benson A. J., Malbon R., Helly J. C., Frenk C. S., Baugh C. M., Cole S., Lacey C. G., 2006, MNRAS, 370, 645
Bruzual G., Charlot S., 2003, MNRAS, 344, 1000
Carlberg R. G., 1984, ApJ, 286, 403
Cowie L. L., Songaila A., Hu E. M., Cohen J. G., 1996, AJ, 112, 839
De Lucia G. et al., 2004, APJ, 610, L77
De Lucia G. et al., 2007, MNRAS, 374, 809
de Propris R., Stanford S. A., Eisenhardt P. R., Dickinson M., Elston R., 1999, AJ, 118, 719
Dressler A. et al., 1997, ApJ, 490, 577
Ebeling H., Edge A. C., Allen S. W., Crawford C. S., Fabian A. C., Huchra J. P., 2000, MNRAS, 318, 333
Ebeling H., Edge A. C., Henry J. P., 2001, ApJ, 553, 668
Ebeling H., Barrett E., Donovan D., Ma C.-J., Edge A., van Speybroeck L., 2007, ApJ, 661, L33
Ebeling H., Voges W., Bohringer H., Edge A. C., Huchra J. P., Briel U. G., 1996, MNRAS, 281, 799
Ellis S. C., Jones L. R., 2004, MNRAS, 348, 165
Gilbank D. G., Balogh M. L., 2008, MNRAS, 385, L116
Gladders M. D., Lopez-Cruz O., Yee H. K. C., Kodama T., 1998, ApJ, 501, 571
Gladders M. D., Yee H. K. C., 2000, AJ, 120, 2148
Jones L. R., Scharf C., Ebeling H., Perlman E., Wegner G., Malkan M., Horner D., 1998, ApJ, 495, 100
Kauffmann G., Charlot S., 1998, MNRAS, 294, 705
Kim R. S. J., Annis J., Strauss M. A., Lupton R. H., 2002, in Borgani S., Mezzetti M., Valdarnini R., eds, ASP Conf. Ser. Vol. 268, Tracing Cosmic Evolution with Galaxy Clusters. Astron Soc. Pac., San Francisco, p. 395

Kodama T., Arimoto N., 1997, A&A, 320, 41
Kodama T. et al., 2004, MNRAS, 350, 1005
Larson R. B., Tinsley B. M., Caldwell C. N., 1980, ApJ, 237, 692
Lawrence A. et al., 2007, MNRAS, 379, 1599
Lopez-Cruz O., 1997, PhD thesis, University of Toronto
Lopez-Cruz O., Barkhouse W. A., Yee H. K. C., 2004, ApJ, 614, 679
Mei S. et al., 2006, ApJ, 644, 759
Pimbblet K. A., Smail I., Edge A. C., Couch W. J., Hely E. O., Zabludoff A. I., 2001, MNRAS, 327, 588
Pimbblet K. A., Smail I., Edge A. C., O'Hely E., Couch W. J., Zabludoff A. I., 2006, MNRAS, 366, 645
Popesso P., Biviano A., Böhringer H., Romaniello M., Voges W., 2005, A&A, 433, 431
Porter S. C., Raychaudhury S., Pimbblet K. A., Drinkwater M. J., 2008, MNRAS, 388, 1152
Scharf C. A., Jones L. R., Ebeling H., Perlman E., Malkan M., Wegner G., 1997, ApJ, 477, 79
Skrutskie M. F. et al., 2006, AJ, 131, 1163
Smail I., Edge A. C., Ellis R. S., Blandford R. D., 1998, MNRAS, 293, 124
Smith R. J. et al., 2008, MNRAS, 386, 96
Springel V. et al., 2005, Nat, 435, 629
Stanford S. A., Eisenhardt P. R., Dickinson M., 1998, ApJ, 492, 461
Stott J. P., Smail I., Edge A. C., Ebeling H., Smith G. P., Kneib J.-P., Pimbblet K. A., 2007, ApJ, 661, 95
Stott J. P., Edge A. C., Smith G. P., Ebeling H., Swinbank A. M., 2008, MNRAS, 384, 1502
Swinbank A. M. et al., 2007, MNRAS, 379, 1343
Tamura N., Ohta K., 2000, AJ, 120, 533
Visvanathan N., Sandage A., 1977, ApJ, 216, 214
Wake D. A., Collins C. A., Nichol R. C., Jones L. R., Burke D. J., 2005, ApJ, 627, 186
Worthey G., Trager S. C., Faber S. M., 1995, in Buzzoni A., Renzini A., Serrano A., eds, ASP Conf. Ser. Vol. 86, Fresh Views of Elliptical Galaxies. Astron. Soc. Pac., San Francisco, p. 203

This paper has been typeset from a TEX/LATEX file prepared by the author.